https://doi.org/10.5194/egusphere-2026-4098
Preprint. Discussion started: 31 August 2026

Development of the Asian Dust Emission Scheme Version 1.0 (ADES v1.0) for East Asia in WRF-Chem v3.9.1 Constrained by *in situ* Tower Observations

Jae-Hyeong Lee[1,2], Sang-Hyun Lee[1,2,*], Moon-Soo Park[3], Hongsheng Zhang[4]

[1]Department of Atmospheric Science, Kongju National University, Gongju, Republic of Korea
[2]Particle Pollution Research and Management Center, Kongju National University, Gongju, Republic of Korea
[3]Department of Climate and Environment, Sejong University, Seoul, Republic of Korea
[4]Laboratory for Climate and Ocean-Atmosphere Studies, Department of Atmospheric and Oceanic Sciences, School of Physics, Peking University, Beijing 100871, PR China

Correspondence to: Sang-Hyun Lee (sanghyun@kongju.ac.kr)

Abstract. Accurate modelling of natural dust emissions in East Asia remains challenging mainly due to complex surface conditions. Previous dust schemes often exhibited diverse sensitivities of dust emission flux to friction velocity and relied heavily on highly uncertain topography-based static source strength functions (S). To overcome these limitations, we developed the Asian Dust Emission Scheme version 1.0 (ADES v1.0), a new semi-empirical dust emission scheme optimized for the East Asian region, directly constrained by *in situ* micrometeorological and multi-level PM_{10} observations obtained from the Horqin Desert area. Rather than relying on simple log-linear regression between dust emission flux and friction velocity, the new scheme introduces a refined dust flux formulation by directly optimizing it against field measurements. This yields a robust relationship where the dust emission flux is proportional to the friction velocity raised to the power of 1.72 ($F \propto u_*^{1.72}$), which contrasts with the conventional third to fourth power relationships. Furthermore, the new scheme completely eliminates the conventional dependence on static source strength functions (S) and incorporates dynamic surface condition properties, such as soil freezing, vegetation cover, and snow fraction, as direct reduction factors that better reflect the complex land conditions of East Asia. The new scheme was implemented into the three-dimensional WRF-Chem model (version 3.9.1) along with the updated dust source region map and evaluated against two distinct Asia dust events: a wintertime event in February 2015 and a springtime event in March 2021. The control simulation utilizing the existing schemes (GOCART, AFWA, and UC schemes) exhibited severe underestimation or overestimation depending on the friction velocity and soil texture configurations. Conversely, the new semi-empirical scheme significantly reduced these systematic biases, demonstrating substantially improved performance in capturing both the onset and magnitude of dust outbreaks. Strikingly, the new scheme effectively suppressed the chronic overestimation of PM_{10} concentrations under strong wind conditions by accounting for the realistic gentler slope of dust emission fluxes, while successfully capturing the long-range transport of dust plumes to downwind regions, including the Korean Peninsula. These findings underscore that incorporating direct in situ tower constraints and dynamic source maps into numerical models is essential for mitigating the long-lasting uncertainties in regional dust simulations over East Asia.

https://doi.org/10.5194/egusphere-2026-4098
Preprint. Discussion started: 31 August 2026

1 Introduction

Mineral dust aerosols play a crucial role in the Earth's climate system by modulating the radiative energy balance through the absorption and scattering of solar and terrestrial radiation (e.g., Park and In, 2003; Huang et al., 2014; Chen et al., 2018). Beyond their climatic impacts, dust particles significantly degrade regional air quality and pose several risks to human health as well as agricultural and industrial activities in downwind regions (e.g., Shinn et al., 2000; Yuan and Zhang, 2006; Wang et al., 2021). East Asia, which encompasses vast arid and semi-arid regions such as the Gobi and Taklimakan deserts, is one of the most prominent global sources of atmospheric dust aerosols (Sun et al., 2001; Ginoux et al., 2012). Dust outbreaks in this region exhibit distinct seasonal variations, primarily peaking during spring when strong cold fronts associated with mid-latitude cyclones sweep across erodible land surfaces (Zhou and Zhang, 2003; Zhou et al., 2024). In downwind regions, recent observations indicate an increasing frequency of wintertime dust events reaching the Korean Peninsula (NIMS, 2024).

Numerical modelling utilizing three-dimensional chemical transport models (CTMs), such as the Weather Research and Forecasting model coupled with Chemistry (WRF-Chem), is essential for forecasting dust transport and quantifying its regional impacts (e.g., Uno et al., 2006). Various dust emission schemes have been developed and implemented into the CTMs over the past few decades under different representations of physical processes using field observations and wind tunnel experiments over idealized soil surfaces (Bagnold, 1941; Woodruff and Siddoway, 1965; White, 1979; Iversen and White, 1982; Westphal et al., 1987; Marticorena and Bergametti, 1995; Alfaro et al., 1997; Kok et al., 2014). However, accurate simulation of dust emission fluxes in East Asia remains highly uncertain. This limitation stems from the diverse mathematical formulations and inherent empirical parameters embedded within existing dust emission schemes (Lee and Lee, 2022). Widely implemented schemes include the physically-based University of Cologne (UC) schemes (Shao, 2001, 2004; Shao et al., 2011), the empirical Mineral Dust Entrainment and Deposition (DEAD) scheme (Zender et al., 2003), the Goddard Global Ozone Chemistry Aerosol Radiation and Transport (GOCART) scheme (Ginoux et al., 2001), the Asian Dust Aerosol Model (ADAM) (Park and In, 2003; Park et al., 2010a), and the semi-empirical Air Force Weather Agency (AFWA) scheme (LeGrand et al., 2019). These schemes often demonstrate divergent sensitivities of dust emission fluxes to surface friction velocity (u_*) under different regions and dust intensities (e.g., Su and Fung, 2015; Fountoukis et al., 2016; Kim et al., 2021). Consequently, these models frequently under- or overestimate observed PM_{10} concentrations during strong wind events (Su and Fung, 2015; Fountoukis et al., 2016; Yuan et al., 2019; Zhao et al., 2020; Han et al., 2021; Kim et al., 2021; Lee and Lee, 2022).

A major source of systematic error in conventional schemes is their strong reliance on a static topography-based dust source strength function (S) to determine potential dust erodibility (Ginoux et al., 2001). While this prescribed function effectively identifies persistent, low-lying hydrologic basins like the Taklimakan Desert, it inherently fails to capture the highly dynamic surface conditions of other prominent East Asian source regions, such as the Mongolian Plateau and the Horqin Desert. In these areas, erodibility varies dramatically in response to transient land surface changes, including seasonal vegetation growth, intermittent snow cover, and seasonal soil freezing-thawing cycles (Lee and Park, 2006; NIMR, 2008; Park et al., 2010a; Lee et al., 2019). High-latitude deserts experience prolonged sub-zero temperatures during winter, leading to topsoil freezing that strongly suppresses dust emissions-a physical constraint that static geographical maps cannot resolve (Han et al., 2011; Wang et al., 2014).

Furthermore, existing schemes are critically sensitive to prescribed soil texture configurations and particle size distributions (Lee and Lee, 2022). Physics-based schemes require highly resolved data on minimally and fully disturbed soil particle sizes to simulate complex saltation bombardment and aggregate disintegration processes (Shao, 2001, 2004). Unfortunately, such detailed soil metrics are rarely available with high spatial accuracy across expansive deserts, leading to unstable model responses when shifting between basic soil classes (e.g., sand vs. loamy sand).

To resolve these limitations, we propose a new semi-empirical dust emission scheme optimized specifically for the East Asian region. The foundational relationship between dust emission flux and surface friction velocity was directly constrained and optimized utilizing unique comprehensive datasets collected from a micrometeorological tower deployed

https://doi.org/10.5194/egusphere-2026-4098
Preprint. Discussion started: 31 August 2026

within an East Asian dust source region. Rather than extrapolating ideal laboratory wind-tunnel parameters or relying on simple linear regressions, the proposed formulation directly parameterizes bulk vertical dust fluxes based on actual *in situ* desert observations. In addition, the new scheme completely eliminates the dependence on topography-based source strength functions. Instead, it incorporates monthly varying dynamic dust source maps derived from a multi-satellite detection framework (Lee et al., 2025). Surface constraints unique to East Asian high-latitude geography are explicitly integrated into the bulk flux calculations based on gravimetric soil moisture cohesion (Fécan et al., 1999), vegetation aerodynamic drag effect (Raupach, 1992), snow cover fraction (Kurosaki and Mikami, 2004), and topsoil freezing (Lee and Park, 2006).

The primary objectives of this study are twofold: (1) to present the observation-constrained new semi-empirical dust emission scheme (ADES v1.0), and (2) to evaluate its implementation within the WRF-Chem model against two severe dust events in winter and spring. The remainder of this paper is organized as follows: Section 2 details the methodology for estimating dust emission fluxes using multi-level tower measurements and describes the verification approach. Section 3 formulates the equations of the new semi-empirical dust emission scheme. Section 4 presents the evaluation of the stand-alone version comparing it against previous schemes. Section 5 describes the integration of the newly developed dust emission scheme into the WRF-Chem model and evaluates its performance for severe wintertime and springtime dust events. Finally, our conclusions are presented in Section 6.

2 Observational Data and Dust Flux Estimation

2.1 Observation site and measurements

The observation site is located at the Horqin Desert in Naiman (42° 56′N; 120° 42′E, 367 m) in Inner Mongolia, approximately 500 km northeast of Beijing, China (Fig. 1). Geographically, the Horqin Desert is a major source region for Asian dust affecting the Korean Peninsula, situated closer than other major sources like the Gobi or Taklimakan Deserts. The site is characterized by semi-arid climate condition with an annual precipitation of about 372 mm and potential evaporation of approximately 1935 mm (Imagawa et al., 2006; Wang et al., 2013; Zhao et al., 2007; Ju et al., 2018). The landscape is dominated by sandy soil containing clay (Park et al., 2011a), with open shrublands such as *Caragana microphylla* and *Salix gordejevii* distributed along a gradual slope (Zhao et al., 2007).

The 20-m triangular lattice mast at the site is equipped with micrometeorological and dust concentration instruments. At a height of 8 m, a sonic anemometer measures three-dimensional turbulent wind components (CSAT3, Campbell Sci. Inc.). Vertical profiles of air temperature, relative humidity (HMP45C, Campbell Sci. Inc.), and wind speed (010C, Met One Instruments Inc.) are measured at heights of 2, 4, 8, and 16 m. In addition, soil temperature (CS107, Campbell Sci. Inc.) and moisture (CS616, Campbell Sci. Inc.) were measured at depths of 5, 20 and 50 cm, while surface radiation (LI200X, Campbell Sci. Inc.) and atmospheric pressure (PTB110, Vaisala Co.) were collected at a height of 2 m. Dual-level measurements of PM_{10} concentrations (FH62C14, Thermo Sci.) at 3 m and 15 m heights were designed to estimate vertical dust fluxes based on the gradient method. Two beta gauges operated at a flow rate of 1000 l h^{-1} and were calibrated every six months (Park et al., 2010b; Park et al., 2011a; Park et al., 2011b; Park et al., 2016a).

Data were collected for approximately one year from 1 August 2011 to 28 August 2012. Raw data were sampled at 10 Hz, and the data were aggregated into 10-minute average dataset after conducting subsequent quality control processes (e.g., removing short-lived spikes, instrumental errors) (Park and Park, 2006; Park et al., 2011a; Park et al., 2016a). All measured 10-minute average data were smoothed by taking a running mean to obtain 1-hour mean data for analysis. From the data, a 'dust event' was strictly defined as a period when the PM_{10} concentration at 3 m height exceeded 200 $\mu g\ m^{-3}$. Based on this criterion, 232 hours of data (approximately 3.2% of the total period) were identified as dust events, with the highest frequency occurring in spring (~50%).

https://doi.org/10.5194/egusphere-2026-4098
Preprint. Discussion started: 31 August 2026

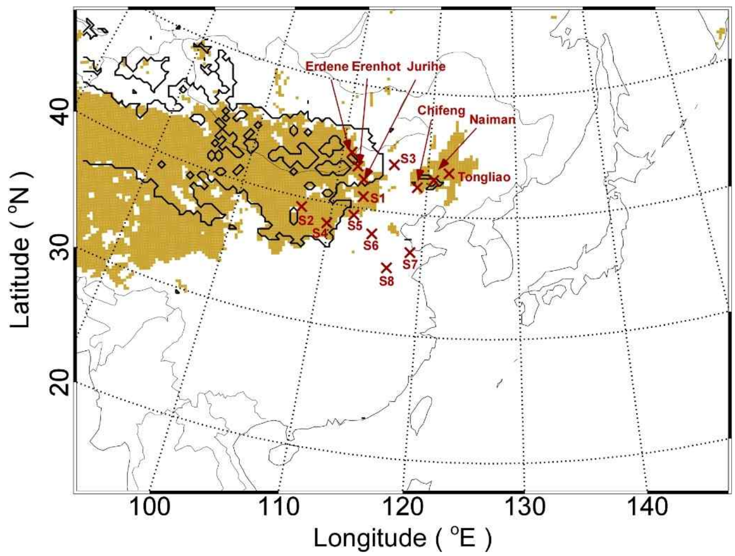

Figure 1. Natural dust source regions in East Asia. The yellow shading is the updated dust source region map (March), and the contour lines represent the dust source regions (EROD) of the WRF-Chem model. Red symbols are measurement sites used to validate the new dust emission scheme.

2.2 Derivation of dust emission fluxes

Dust emission fluxes were derived using the gradient method based on the vertical difference in PM_{10} concentrations measured at the tower. Using the dust concentrations at $z_1 = 3$ m and $z_2 = 15$ m, along with the eddy diffusivity calculated at 8 m, the dust emission flux (F_c) is estimated as follows:

$$F_c = -K_z \frac{\Delta C}{\Delta z}, \quad (1)$$

where ΔC is the difference in dust concentration between the two heights and K_z is the vertical eddy diffusivity at height z, defined as:

$$K_z = \frac{k(z-d)u_*}{\Phi_h}. \quad (2)$$

Here, $k(= 0.41)$ is the von Karman constant, d is the zero-plane displacement height, u_* is the friction velocity, and Φ_h is the dimensionless stability correction function for heat. In this study, we utilized the universal function by Dyer (1974) and Park et al. (2011a) as follows:

$$\Phi_h = \begin{cases} \left(1 - 15\frac{z}{L}\right)^{-\frac{1}{2}} & for\ \frac{z}{L} < 0 \\ 1 + 5\frac{z}{L} & for\ \frac{z}{L} > 0 \end{cases}. \quad (3)$$

The Obukhov length scale (L) is calculated using the mean air temperature ($\overline{T}$), gravitational acceleration (g), and kinematic heat flux ($\overline{w'T'}$) as follows:

$$L = \frac{\overline{T}u_*^3}{kg\overline{w'T'}}. \quad (4)$$

Figure 2 shows the time series of dust emission fluxes estimated from the micrometeorological and dust concentration measurements. The 25 to 75% interquartile range of dust emission fluxes that occurred during the dust events (232 hours) appear in the range of approximately 1.0 to 10.6 μg m^{-2} s^{-1}. The derived dust emission fluxes showed a strong seasonal variability, peaking in late April, which is collocated with the maximum friction velocity (up to 1.81 m s^{-1}) and near-ground PM_{10} concentration (~2000 μg m^{-3}).

https://doi.org/10.5194/egusphere-2026-4098
Preprint. Discussion started: 31 August 2026

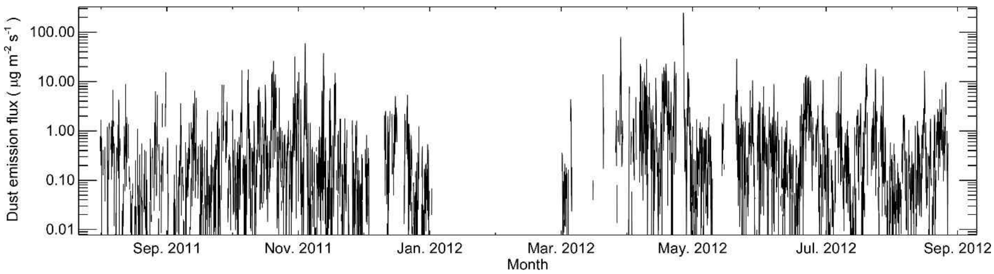

Figure 2. Time series of dust emission flux estimated from the Naiman monitoring tower measurements for the period August 1, 2011, to August 28, 2012.

3 Asian Dust Emission Scheme version 1.0 (ADES v1.0)

A new semi-empirical dust emission scheme was developed based on the framework of the AFWA scheme (Marticorena and Bergametti, 1995; LeGrand et al., 2019). This development incorporates the performance characteristics and limitations identified in previous sensitivity simulations of dust schemes over the East Asian region (Su and Fung, 2015; Zhao et al., 2020; Kim et al., 2021; Lee and Lee, 2022). The new scheme is characterized by establishing an advanced empirical relationship between dust emission flux and friction velocity, achieved by directly optimizing the comprehensive flux calculation equation against multi-level tower observations in the Horqin Desert. Furthermore, the new model completely eliminates the conventional dependence on topography-based static dust source strength functions.

Due to the high sensitivity of physically based schemes (e.g., UC schemes) to soil particle size distributions in the saltation and disintegration processes (Lee and Lee, 2022), the basic mass fractions of clay, silt, and sand were adopted to represent the soil particle size distribution in the new scheme. To support the accurate application of the optimized flux relationship, we additionally improved the calculation process of the threshold friction velocity. This comprehensively modified threshold dynamically accounts for region-specific constraints such as soil moisture cohesion, vegetation aerodynamic drag effect, and snow cover fraction, which act as critical environmental reduction factors suppressing dust outbreaks. These physical constraints are explicitly included because East Asian dust source regions are distributed at relatively high latitudes, where wintertime surface conditions strongly control dust availability. The new semi-empirical dust emission scheme was initially developed and evaluated as a stand-alone box model before its subsequent three-dimensional integration.

3.1 Formulation of the new dust emission scheme

3.1.1 Bulk dust emission flux

The primary objective of the dust emission scheme is to calculate the bulk vertical dust emission flux (F) that is integrated into the three-dimensional atmospheric model. In the new semi-empirical scheme, F is calculated from the sandblasting process driven by the horizontal saltation of soil particles (Marticorena and Bergametti, 1995). To explicitly account for the complex surface conditions of East Asia (Lee and Park, 2006), the final dust emission flux is calculated by applying a critical reduction factor to the optimized maximum flux:

$$F = R_{sol} \cdot \beta \cdot F_d, \tag{5}$$

where F_d is the total horizontal saltation flux (detailed in Section 3.1.2), β is the sandblasting efficiency, and R_{sol} is the soil-freezing reduction factor. β depends on the clay content and ranges from 1.0×10^{-6} to 1.36×10^{-6} cm^{-1}.

In previous parameterizations such as the AFWA scheme, a topography-based dust source strength function (S) is applied to represent the potential of dust availability in the calculation of bulk dust emission fluxes (Ginoux et al., 2001; LeGrand et al., 2019). However, the spatial distribution of this prescribed function exhibits inherent limitations in accurately representing actual dust source regions in East Asia. Previous studies have reported significant underestimation in simulated

https://doi.org/10.5194/egusphere-2026-4098
Preprint. Discussion started: 31 August 2026

dust emission fluxes due to the dependence on the artificially low dust source strength assigned to this region (Su and Fung, 2015; Lee and Lee, 2022). Therefore, the new dust emission scheme completely eliminates the dependence on the static source strength function.

Because dust source regions in East Asia are distributed at relatively high latitudes, dust occurrence is strongly influenced by topsoil freezing (Han et al., 2011; Wang et al., 2014). The impact of soil freezing (R_{sol}) is parameterized to decrease linearly based on the ground temperature (T_g) using thresholds derived from previous regional observations (Lee and Park, 2006; NIMR, 2008):

$$R_{sol} = \begin{cases} 1 & , T_g > -5℃ \\ 1 + \frac{T_g}{100} & , T_g \le -5℃ \end{cases}, \quad (6)$$

yielding a 5% to 30% reduction for ground temperatures between –5°C and –30°C.

3.1.2 Horizontal saltation flux

Total horizontal saltation flux (F_d) represents the mass of soil particles lifted from the ground by wind drag. The saltation process is triggered when the surface friction velocity (u_*) exceeds the comprehensively modified threshold friction velocity ($u_{*,t}$). Because wind drag force is insufficient to lift soil particles infinitely, their vertical motion is typically limited to a height of about 1 m. The soil particle size-dependent saltation flux is calculated based on the formulation by Marticorena and Bergametti (1995) and LeGrand et al. (2019) as follows:

$$F_d = \begin{cases} \sum_d \alpha_{new} \frac{\rho_a}{g} u_*^{\beta_{new}} \left(1 + \frac{u_{*,t}(d,\theta,\lambda)}{u_*}\right)\left(1 - \frac{u_{*,t}^2(d,\theta,\lambda)}{u_*^2}\right) dS_{rel}(d), & u_* > u_{*,t}(d,\theta,\lambda) \\ 0 & u_* \le u_{*,t}(d,\theta,\lambda) \end{cases}, \quad (7)$$

where α_{new} is the empirical proportionality constant, β_{new} is the power of the friction velocity, ρ_a is the atmospheric density, and g is the gravitational acceleration. $dS_{rel}(d)$ is the surface area distribution relative to the total basal surface area of the soil, representing the relative contribution to the total horizontal saltation flux.

The sensitivity of F_d to friction velocity is strictly governed by the α and β parameters. In the AFWA scheme, 1.0 is adopted as the proportionality constant (α), and 3.0 is adopted as the power of friction velocity (β). Previous studies have parameterized this relationship using various exponents ($F \propto u_*^n$), typically ranging from 2 to 5 (Westphal et al., 1987; Gillette and Passi, 1988; Shao et al., 1993, 1996; Shao, 2001, 2004; Zhang et al., 2008; Park and In, 2003; Fratini et al., 2007; Park et al., 2011a; Park et al., 2016a). This wide range introduces significant uncertainties, frequently leading to an excessive overestimation of dust fluxes under strong winds over East Asia. To resolve this discrepancy, the new scheme completely replaces these conventional values with newly optimized coefficients directly constrained by field measurements (described in Section 3.2).

The relative contribution $dS_{rel}(d)$ is expressed based on the relative surface area of particles with diameter d compared to the total surface area of the soil layer (B_{total}) (Marticorena and Bergametti, 1995):

$$dS_{rel}(d) = \frac{B_s(d)}{B_{total}}, \quad (8)$$

where $B_s(d)$ is the relative surface area for particles of diameter d, defined assuming spherical particles of equal density as:

$$B_s(d) = \frac{dM(d)}{\frac{2}{3}\rho_d d}, B_{total} = \sum_d B_s(d). \quad (9)$$

Here, $dM(d)$ represents the mass contribution of soil particles (clay, silt, and sand) within each size bin, ρ_d is the particle density, and d is the particle diameter. The total saltation flux is obtained by summing the fluxes calculated across all size bins to estimate the aggregate vertical dust emission flux.

https://doi.org/10.5194/egusphere-2026-4098
Preprint. Discussion started: 31 August 2026

3.1.3 Threshold friction velocity

Accurate initiation of saltation flux requires a refined calculation of the threshold friction velocity. Unlike simple formulations that trigger emissions prematurely, $u_{*,t}(d,\theta,\lambda)$ explicitly incorporates East Asian surface constraints. The new semi-empirical threshold is corrected to account for real ground conditions and is expressed as:

$$u_{*,t}(d,\theta,\lambda) = u_{*,t}(d) \times f(\theta) \times f(\lambda) + \Delta u_{*,t}, \qquad (10)$$

where $u_{*,t}(d)$ is the threshold friction velocity for smooth, dry soil without roughness elements, $f(\theta)$ is the soil moisture correction function, $f(\lambda)$ is the roughness correction function, and $\Delta u_{*,t}$ is the threshold increment due to snow cover fraction.

The $u_{*,t}(d)$ is derived from wind tunnel experiments as follows (Iversen and White, 1982; Marticorena and Bergametti, 1995):

$$u_{*,t}(d) = 0.13\left(\left(\frac{\rho_d g d}{\rho_a}\right)^{0.5}\left(1 + \frac{0.006}{(\rho_d g d)^{2.5}}\right)^{0.5}\right) / [1.928(ad^x + b)^{0.092} - 1]^{0.5}, \qquad (11)$$

where the empirical constants are $x = 1.56$, $a = 1331\sigma n^{-x}$, and $b = 0.38$.

To account for actual surface constraints, the soil moisture correction $f(\theta)$ accounts for capillary forces that increase particle cohesion based on gravimetric soil moisture and clay content. Fécan et al. (1999) presented an empirical relationship between soil moisture and clay content obtained from wind tunnel experiments, and is calculated as follows:

$$f(\theta) = \begin{cases} \sqrt{1 + 1.21(\theta_g - \theta'_g)^{0.68}} & ,\theta_g > \theta'_g \\ 1 & ,\theta_g \le \theta'_g \end{cases}, \qquad (12)$$

where θ_g is the weight of soil moisture, θ'_g is the soil moisture that can be absorbed before capillary forcing affects particle separation, and is calculated as:

$$\theta'_g = 0.0014(100c_s)^2 + 0.17(100c_s), \qquad (13)$$

where c_s is the clay content obtained from topsoil (0-30 cm). The weight of soil moisture is calculated from its relationship with volumetric soil moisture as follows:

$$\theta_g = \frac{\theta_v \rho_w}{(2.65 - 0.15c_s)(1-\emptyset)}, \qquad (14)$$

where θ_v is the volumetric soil moisture (m^3 m^{-3}), ρ_w is the water density (=1.0 g cm^{-3}), 2.65-0.15c_s is the soil density, and $\emptyset$ is the soil porosity.

The roughness correction $f(\lambda)$ represents wind momentum absorbed by non-erodible elements using the frontal area index derived from vegetation fraction (Raupach, 1992):

$$r = \sqrt{1 - 0.5\lambda} + \sqrt{1 + 100\lambda}, \qquad (15)$$

where λ is the frontal area index calculated as a function of vegetation fraction (v_f) and is calculated as $\lambda = 0.35\ln(1 - v_f)$. Finally, the snow cover effect $\Delta u_{*,t}$ is incorporated following Kurosaki and Mikami (2004) as follows:

$$\Delta u_{*,t} = \begin{cases} k\frac{0.027 f_s}{\ln z/z_0} & ,f_s > 0 \\ 0 & ,f_s = 0 \end{cases}, \qquad (16)$$

where k is the von Karman constant, f_s is the snow cover fraction, z_0 is the roughness length, and z is the reference height (~10 m). When the snow cover fraction is approximately 10%, the threshold friction velocity increases by approximately 0.015 m s^{-1}.

3.2 Parameter optimization using tower observations

To isolate the fundamental relationship between dust emission flux and friction velocity, the 232 hours of identified dust events from the Naiman monitoring tower were strictly filtered. Periods significantly influenced by transient land surface variations were excluded, thereby minimizing the masking effects of the reduction factors. The remaining 157 hours of pure dust emission flux data were utilized for parameters of the new semi-empirical dust emission scheme. To directly apply the

https://doi.org/10.5194/egusphere-2026-4098
Preprint. Discussion started: 31 August 2026

actual *in situ* measurements from the source region to the new dust emission scheme, the optimal values of α_{new} and β_{new} were determined by identifying the coefficients that yielded the highest correlation between the measured fluxes and the theoretical fluxes calculated using Eq. (5). This approach fundamentally differs from previous studies that simply explored the direct exponential relationship between friction velocity and dust flux using simple linear regression. However, for quantitative comparison with these previous studies, the newly estimated parameter values were also compared with those proposed in the literature (Table 1).

Based on the independent non-linear best-fit curve derived from the filtered monitoring tower data (Fig. 3), we determined a proportionality constant (α_{new}) of 0.18 and a friction velocity exponent (β_{new}) of 1.72. The relations in the previous studies typically reported a steeply increasing dust emission flux with rising friction velocity (Gillette, 1977; Westphal et al., 1987; Fratini et al., 2007; Zhang et al., 2008; Park et al., 2011a; Shao et al., 2011). While traditional parameterizations produce a steeply increasing dust emission flux proportional to the third to fourth power of friction velocity (Table 1), the newly optimized parameterization demonstrates a relatively gentler emission slope (R = 0.61).

This discrepancy is primarily attributed to regression methodologies and the friction velocity ranges. Previous studies were constrained to a lower friction velocity range of 0.01 to 1.20 m s^{-1}, whereas our dataset covers a wider range of 0.03 to 1.81 m s^{-1}. Notably, when limiting our dataset to less than 1.5 m s^{-1}, the derived exponent sharply increased to approximately 4.6. This underscores that traditional models suffer from a severe overestimation pitfall under strong wind conditions due to the uncalibrated extrapolation of lower-wind parameter sets.

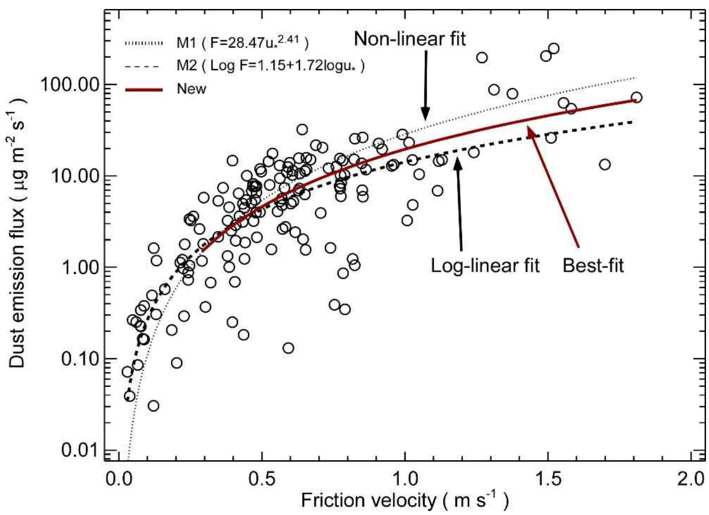

Figure 3. Relationship between dust emission flux and friction velocity. The best-fit relation was found based on filtered data (n = 157) during the dust events period at the Naiman tower in the Horqin Desert.

Table 1. Comparison of fitting coefficients of the flux-friction velocity relation ($F = \alpha u_*^{\beta}$) between dust emission flux and friction velocity obtained in different deserts.

α	β	u_* range (m s^{-1})	Measurement period	Location	Reference
0.01	3.0	0.4~1.1	2 days (30 Apr.-1 May)	Gobi Desert	Judger (2019)
9.50	3.13	0.1~1.2	4 months (Nov. 2007~Mar. 2008)	Horqin Desert	Park et al. (2011a)

https://doi.org/10.5194/egusphere-2026-4098
Preprint. Discussion started: 31 August 2026

52.50	2.93	0.1~1.0	1 month (Mar. 2004)	Hunshandake Desert	Zhang et al. (2008)
4.70	3.36	0.1~0.6	6 days (22~28 May 2005)	Alashan Desert	Fratini et al. (2007)
6.30-10.0	3.7-4.0	0.2~1.1	6 months (Mar.~Apr. 1972-1975)	Eroding fields (Texas)	Gillette (1977)

4 Stand-alone Model Evaluation

4.1 Reference dust emission schemes and experimental setup

To evaluate the new scheme, five widely used dust emission schemes were selected for comparison: UC01, UC04, UC11, GO01, and GA19. The UC (University of Cologne) schemes are physics-based models. The UC01 scheme (Shao, 2001) incorporates detailed physical processes including saltation bombardment and aggregate disintegration. Soil particle size distributions associated with the physical mechanisms are dynamically determined as minimally and fully disturbed particle size distributions according to soil type and soil condition. The UC04 scheme (Shao, 2004) simplified parameters associated with saltation bombardment efficiency of dust particle. While UC01 calculates the dust emission flux from the total saltation flux for each particle size bin, the UC11 scheme (Shao et al., 2011) simplified this process by removing the fully disturbed particle size distribution ($\gamma = 1$) and further simplified the formulation by calculating the dust emission flux directly from the total saltation flux rather than integrating across individual particle size bins. The UC schemes consider dust particle diameters ranging from about 1 to 2000 μm (100 bins). These schemes, as implemented in WRF-Chem, utilize 12 soil texture classes defined based on the United States Department of Agriculture (USDA) classification.

The GO01 (GOCART) scheme (Ginoux et al., 2001) is a simple empirical scheme where the dust emission flux is proportional to the square of 10-m wind speed (u_{10m}) whenever it exceeds a threshold friction velocity ($u_{*,t}$). It also relies on a topography-based source strength function (S) to represent dust particle availability. The GA19 (AFWA) scheme (LeGrand et al., 2019) is a semi-empirical scheme modified from Marticorena and Bergametti (1995). It calculates bulk dust emission flux (F_B) as the product of total horizontal saltation flux (G), sandblasting efficiency (β), and the source strength function (S).

All schemes were conducted using the same meteorological and ground forcing data measured at the Naiman monitoring tower to ensure a consistent comparison. Ground conditions not measured directly at the tower were supplemented with external datasets. Soil texture information, a critical input for dust schemes, was obtained from the Regridded Harmonized World Soil Database (RHWSD, version 1.2) at a horizontal resolution of 0.05°×0.05°. Consistent with previous studies (Park et al., 2011a; Park et al., 2016a), the topsoil (0-30 cm) at the Naiman site is characterized by sand (89%) with minor silt (6%) and clay (5%) fractions for simulations. For the UC schemes, which use 12 predefined soil types, two specific soil textures (sand and loamy sand) that closely represent the site's soil texture configuration were applied in separate runs. For the GO01 and GA19 schemes, the dust source strength function (S) is required (Ginoux et al., 2001; Kim et al., 2017). Following the methodology used in WRF-Chem, S was calculated based on topographic relief using SRTM terrain elevation data with a 3-arcsecond horizontal resolution. The function assumes that potential dust sources are located in basins with low elevation relative to their surroundings:

$$S = \left(\frac{z_{max} - z_h}{z_{max} - z_{min}}\right)^5, \quad (17)$$

where z_{max} and z_{min} are the maximum and minimum elevations within a 10°×10° area, respectively, and z_h is the local elevation.

https://doi.org/10.5194/egusphere-2026-4098
Preprint. Discussion started: 31 August 2026

4.2 Comparison of estimated and simulated dust fluxes

The newly developed dust emission scheme and the five reference schemes were implemented as a stand-alone box model at the Naiman monitoring tower and simulated using the meteorological and surface data monitored during the same period. Dust emission fluxes estimated from the 232-hour dust events identified at the tower were compared and evaluated against the simulated results (Fig. 4). The dust emission fluxes simulated by the new model, which reflects the best-fit relationship optimized directly from the Naiman tower observations, aligned well with the range and distribution of the measured dust emission fluxes (Fig. 4a). In contrast, the five reference dust emission schemes exhibited varying tendencies of severe over- or underestimation. The UC01 and UC04 schemes consistently demonstrated a tendency to underestimate the measured dust emission fluxes over sandy textures, and their overall simulation performances were remarkably similar (Figs. 4b-c). These results are consistent with previously reported evaluations of the dust schemes in the East Asia region using 3-dimensional chemical transport models (Zhao et al., 2020; Lee and Lee, 2022). The simulated dust emission fluxes of UC11 fell within a similar range to the measurements but exhibited an exaggerated sensitivity as the friction velocity increased (Fig. 4d).

Furthermore, the UC schemes showed a significant sensitivity to the 12 soil texture classes (e.g., sand vs. loamy sand). When transitioning from a sand texture to a loamy sand texture, the UC01 and UC04 schemes simulated an explosive increase in dust emission fluxes by more than two orders of magnitude (i.e., a factor of 100), depending on the friction velocity. This extreme variation is attributed to the high sensitivity of the minimally and fully disturbed particle size distributions defined for different soil types. Conversely, under the same loamy sand texture, the UC11 scheme consistently reduced the simulated dust emission fluxes by approximately an order of magnitude (a factor of 10) (Fig. 4d). These wildly fluctuating results suggest that highly accurate, high-resolution soil particle size distribution data are strictly required when applying these physics-based schemes to East Asian deserts. For the empirical GO01 scheme, friction velocity is plotted as a proxy for the 10-m wind speed for consistent comparison. The GO01 scheme consistently overestimated the dust emission fluxes compared to the tower measurements (Fig. 4e), initiating dust emissions even at low friction velocity ranges (< 0.3 m s^{-1}). This overestimation is well-known characteristic of schemes heavily reliant on simple 10-m wind speed and static threshold functions, as reported in previous studies (LeGrand et al., 2019; Zhao et al., 2020; Lee and Lee, 2022). The performance of the semi-empirical GA19 scheme was somewhat similar to the UC11 scheme, demonstrating an increasingly strong sensitivity to dust emissions as friction velocity increased (Fig. 4f). In summary, the dust emission fluxes simulated by the existing reference schemes showed highly unstable sensitivities to soil texture and friction velocity, supporting widespread discrepancies observed in dust concentration validation at different geographical location and dust emission intensities (Kok et al., 2014; Lee and Lee, 2022). By comprehensively mitigating these uncertainties, the new semi-empirical dust emission scheme, grounded in the best-fitting relationships derived directly from monitoring tower data, demonstrates a vastly superior potential to accurately simulate natural dust fluxes occurring in East Asia.

https://doi.org/10.5194/egusphere-2026-4098
Preprint. Discussion started: 31 August 2026

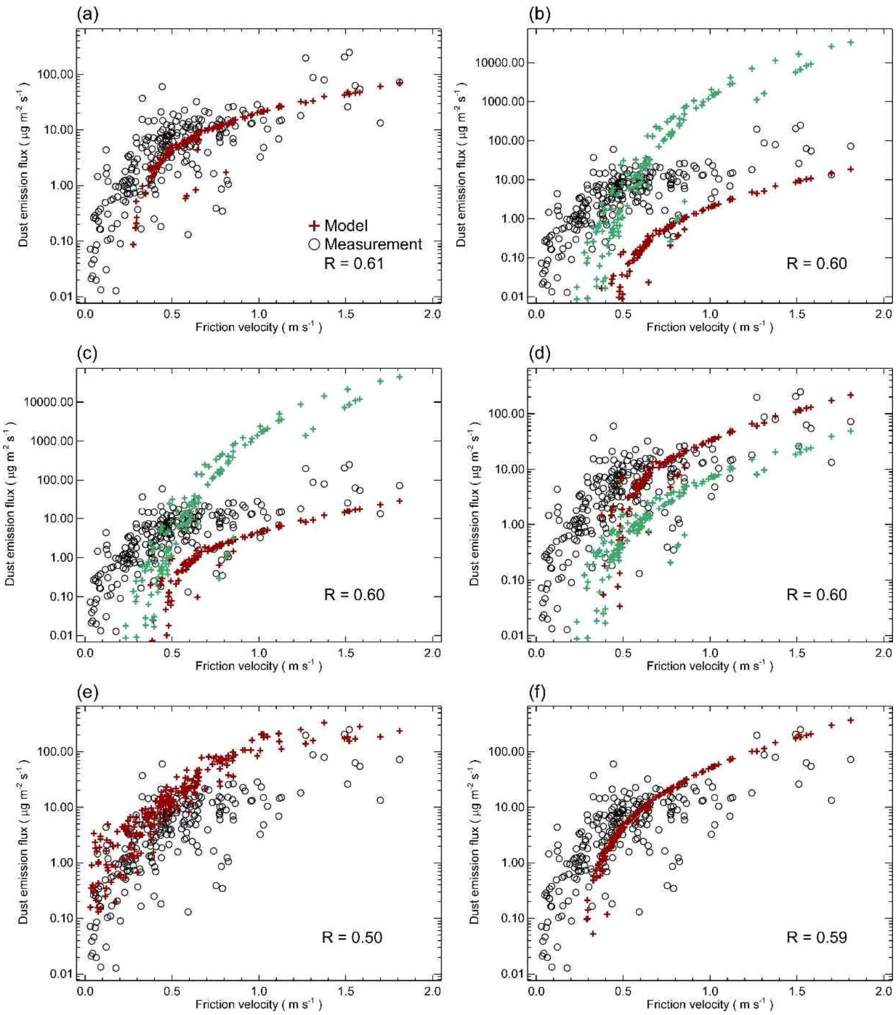

Figure 4. Scatterplot comparison of monitored (black symbols) and simulated (red symbols) dust emission fluxes from Naiman tower and a new dust emission scheme in the Horqin desert, East Asia, during the dust events (n=232). (a) New scheme, (b) UC01, (c) UC04, (d) UC11, (e) GO01, (f) GA19. The green lines and symbols for the UC schemes represent the simulated dust emission flux to the loamy sand texture.

5 Implementation and evaluation in WRF-Chem

5.1 Implementation of the new scheme and dynamic dust source region map

5.1.1 Implementation of the new dust emission scheme in WRF-Chem

The ADES v1.0 scheme was fully integrated into the WRF-Chem model (version 3.9.1). WRF-Chem is an online-coupled modelling system that simultaneously resolves meteorological dynamics and chemical processes, thereby enabling realistic physical feedback mechanisms. To ensure structural consistency and ease of maintenance, the proposed scheme was formulated as an independent module, sharing the architectural framework of existing implemented dust schemes (e.g., GOCART, AFWA, and UC schemes). The core physical parameterizations, including the derivation of dust emission fluxes and application of the soil freezing reduction factor, were encoded within a newly developed source files *Module_new_dust.F* (Fig. 5).

https://doi.org/10.5194/egusphere-2026-4098
Preprint. Discussion started: 31 August 2026

Integrating these modules into the existing WRF-Chem framework required systematic modifications across several core codes. Specifically, the primary chemistry driver (*Chem_driver.F*) and the emission driver (*Emission_driver.F*) were updated to correctly route state variables and subroutine calls. Furthermore, the model registry (*Registry.chem*) was expanded to declare the requisite state variables and new packages, while the compilation dependency file (*Makefile, depend.chem*) was modified to incorporate the new source codes. Ultimately, this comprehensive implementation allows users to seamlessly activate the new dust emission scheme by configuring the namelist parameter *dust_opt = 6*.

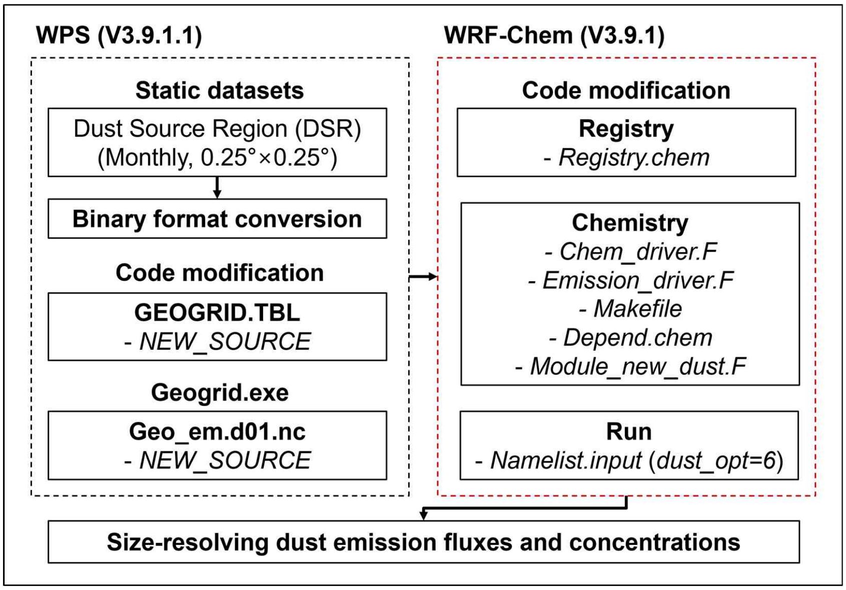

Figure 5. Schematic flowchart illustrating the coupling architecture of the new semi-empirical dust emission scheme within the WRF Pre-processing System (WPS) and the 3-dimensional WRF-Chem model configuration.

5.1.2 Implementation of the new dust source region map in WPS

The new semi-empirical dust emission scheme incorporates monthly dust source regions identified using the dynamic dust source region detection method proposed by Lee et al. (2025) (Fig. S1). Unlike conventional dust source regions estimated based solely on static land-cover classifications, this dust source region detection method integrates satellite and ground-based measurements to identify spatiotemporal variations in natural dust source region based on three criteria (vegetation, snow cover, and land cover) and empirical thresholds for the vegetation bareness index and the snow cover index. It outperforms existing satellite- or ground-based methods in detecting temporal variations and spatial distributions of natural dust sources, making it particularly advantageous for identifying dust source regions with short vegetation and partial snow cover.

To implement this dynamic dust source region map into the WRF-Chem modelling framework, the static information required to run the new dust emission scheme was processed through the WRF Pre-Processing System (WPS). The updated monthly dust source region map dataset, with a horizontal resolution of 0.25° × 0.25°, was converted into the standard binary format compatible with WPS using a customized Fortran routine. Subsequently, the *GEOGRID.TBL* configuration file was modified to define a new land-surface variable designated as *NEW_SOURCE*, detailing its data pathway, interpolation method, and processing priority. By executing the *geogrid.exe* program, these monthly spatial distributions are interpolated directly onto the model grid (*geo_em.d01.nc*), establishing a dynamic initialization field that continuously updates monthly variations in surface conditions.

Crucially, this updated map provides a more comprehensive representation of natural dust sources. In addition to major arid regions such as the Gobi and Taklimakan deserts, it explicitly resolves previously underrepresented areas, including

https://doi.org/10.5194/egusphere-2026-4098
Preprint. Discussion started: 31 August 2026

the Tibetan Plateau, the Manchurian Plain, and vast expanses across Central Asia (e.g., the Balkhash Desert and regions surrounding the Caspian Sea in Kazakhstan and Uzbekistan). By capturing these critical source regions, the updated WPS framework fundamentally resolves the spatial limitations of conventional static maps, enabling more physically robust simulations of Asian dust transport (Lee et al., 2025).

5.2 Asian dust events selection and experimental setup

5.2.1 Asian dust events selection

Springtime and wintertime Asian dust events account for approximately 80-90% of dust occurrences in the East Asia region (Zhou and Zhang, 2003; NIMS, 2015). The wintertime Asian dust event that occurred in the Gobi Desert in February 2015 was selected to investigate whether the limitations of existing dust schemes could be improved (Lee and Lee, 2022). During this event, a strong cold front accompanied by an intense low-pressure system swept across the Gobi Desert, triggering severe dust outbreaks with wind speeds exceeding 15 m s^{-1} (Fig. S2). This case serves as an ideal baseline for evaluating scheme sensitivities under conditions of low temperature, low soil moisture, and freezing topsoil. A detailed description of the wintertime Asian dust event is otherwise documented in Lee and Lee (2022).

A springtime Asian dust event that originated in inland Mongolia and the Gobi Desert from 26 to 28 March 2021 was selected to evaluate the dust simulation performance of the new dust emission scheme (Fig. S3). Asian dust was initially observed in inland Mongolia at 18:00 UTC on March 26 (Figs. S3a-b). The dust plume was subsequently transported southeastward in the wake of a low-pressure system toward eastern Mongolia and the Inner Mongolia Plateau at 12:00 UTC on March 27 (Figs. S3c-d). By 12:00 UTC on March 28, Asian dust was observed near the Shandong Peninsula and Liaoning province in China (Figs. S3e-f). At 15:00 UTC on March 28, an influx of Asian dust was observed over Baengnyeongdo island in South Korea. Because this event originated deep in inland Mongolia, its transport to the Korean Peninsula took longer compared to the wintertime event. During the dust event, high PM_{10} concentrations (~1400 µg m^{-3}) were observed in the west sea of the Korean Peninsula (Kim et al., 2022).

5.2.2 Experimental setup

In this study, the WRF-Chem model (version 3.9.1) was utilized to simulate the selected wintertime and springtime Asian dust events. The simulation domain was configured to cover the entire East Asian dust source region, including the Gobi and Inner Mongolia deserts, using a horizontal grid of 180 × 133 mesh with a grid spacing of 32.4 km. The vertical grid comprises 55 layers extending from a lowest layer depth of approximately 27 m up to a model top of 50 hPa (~20 km), with 17 layers densely allocated within the lowest 1 km to accurately resolve the atmospheric boundary layer (ABL). The physical and chemical configurations are identical to those validated in Lee and Lee (2022). The Regional Atmospheric Chemistry Mechanism (RACM) (Stockwell et al., 1997) and the GOCART scheme (Chin et al., 2000; Ginoux et al., 2001) were used for gaseous and aerosol chemical processes, respectively. Anthropogenic emissions were processed using the Model Inter-Comparison Study for Asia 2010 (MICS-Asia 2010) inventory (Carmichael et al., 2002; Li et al., 2017), while biogenic emissions were provided by the Model of Emissions of Gases and Aerosols from Nature (MEGAN-2) module (Guenther et al., 2006). Direct and indirect physical interactions of aerosols were deactivated to ensure that the simulated meteorological fields remained identical across all sensitivity experiments. National Centers for Environmental Prediction-Final Analysis (NCEP-FNL) global analysis data (1° × 1° horizontal resolution, 6-h intervals) were used for meteorological initial and boundary conditions. The simulated air temperature and specific humidity above the ABL were nudged to the global analysis fields using the four-dimensional data assimilation (4DDA) technique. However, for soil moisture, we applied the Global Land Data Assimilation System (GLDAS) dataset instead of NCEP-FNL.

Figure 6 shows the spatial distribution of the volumetric soil moisture content applied in the WRF-Chem model. The NCEP-FNL data exhibited a wet bias, with about 90% of the grids showing soil moisture up to 0.3 m^3 m^{-3}. In contrast, GLDAS

https://doi.org/10.5194/egusphere-2026-4098
Preprint. Discussion started: 31 August 2026

indicated that approximately 95% of the area had soil moisture below 0.2 m³ m⁻³. A comparison with in situ measurements from the International Soil Moisture Network (ISMN) near the dust source regions showed values ranging from 0.1 to 0.12 m³ m⁻³, which aligned well with the GLDAS data (Fig. S4). Considering these results and previous findings that FNL reanalysis data lack accuracy for soil moisture in China (Dy and Fung, 2016), GLDAS soil moisture was adopted as the initial condition to properly evaluate the dust emission schemes.

To comparatively evaluate the performance of the newly developed semi-empirical scheme, five existing WRF-Chem dust emission schemes were also applied: UC01 (Shao, 2001), UC04 (Shao, 2004), UC11 (Shao et al., 2011), GO01 (Ginoux et al., 2001), and GA19 (LeGrand et al., 2019) (Table 2). Consequently, six independent simulations were conducted for each dust event. The selected dust events featured low precipitation (<0.5 mm) and minimal vegetation/snow cover impacts. For the wintertime event, the simulation period spanned from 00:00 UTC on February 15 to 00:00 UTC on February 24, 2015, with analyses focusing on February 20–24. For the springtime event, the model was integrated from 00:00 UTC on March 20 to 00:00 UTC on April 1, 2021, and data from March 26 to March 30 were analyzed, treating the initial days as a spin-up period (Lee et al., 2015).

The performance of the simulated dust emissions was rigorously evaluated using ground-based PM_{10} concentrations. Within the source regions, we utilized hourly air quality data from stations operated by China's Ministry of Ecology and Environment (MEE), which are widely distributed across the Taklimakan Desert, the Gobi Desert, the Loess Plateau, and the Manchurian Plain (Fig. 1). Additionally, PM_{10} concentrations measured at a 3-m height from monitoring towers in Erdene (Mongolia) and Naiman (China) were used.

Table 2. Experimental design for springtime and wintertime Asian dust simulation using the WRF-Chem dust emission schemes along with the new dust emission scheme.

Experiment name	Dust scheme	Model option	Reference
New	New	Dust_opt=6	This study
UC01	UC	Dust_opt=4, Dust_scheme=1	Shao (2001)
UC04	UC	Dust_opt=4, Dust_scheme=2	Shao (2004)
UC11	UC	Dust_opt=4, Dust_scheme=3	Shao et al. (2011)
GO01	GOCART	Dust_opt=1	Ginoux et al. (2001)
GA19	AFWA	Dust_opt=3	LeGrand et al. (2019)

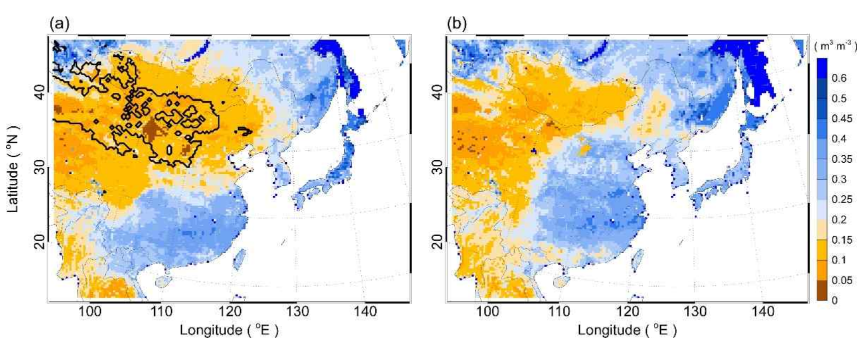

https://doi.org/10.5194/egusphere-2026-4098
Preprint. Discussion started: 31 August 2026

Figure 6. Spatial distribution and histogram distribution of GLDAS (Global Land Data Assimilation System) soil moisture (0–10 cm) applied to the WRF-Chem model for (a) February 2015 and (b) March 2021. The contour line represents the dust source area defined in the WRF-Chem model.

5.3 Comparison of simulated spatial dust emission fluxes

Figure 7 compares the spatial distribution of the averaged dust emission fluxes over the three-day wintertime Asian dust event from February 20 to 23, 2015. During the severe event, the newly developed scheme successfully simulated physically realistic dust emission fluxes, with an average dust emission flux of 40 μg m^{-2} s^{-1} (maximum of ~260 μg m^{-2} s^{-1}) in the primary dust source region (Fig. 7a). Crucially, by utilizing the dynamically updated dust source region map and optimized parameters, the new scheme concentrated intense emissions correctly over the Mongolian Plateau while effectively restraining the unrealistic spatial expansion of dust emissions. In contrast, the previous schemes exhibited extreme structural biases. The UC01 and UC04 schemes showed extreme overestimations (averages of 89 and 104 μg m^{-2} s^{-1}, respectively) and erroneously spread intense fluxes over the northern China (maximum of 2962 and 3528 μg m^{-2} s^{-1}, respectively) due to their strong sensitivity to low soil moisture (Figs. 7b-c). Conversely, the UC11, GO01, and GA19 schemes failed to simulate the event's intensities, producing horizontally uniform and severely underestimated the dust fluxes averaging only 2 to 13 μg m^{-2} s^{-1} (Figs. 7d-f). The new scheme realistically bridged this gap, avoiding both the severe overestimations of UC01 and UC04 and the weak underestimation of UC11, GO01, and GA19.

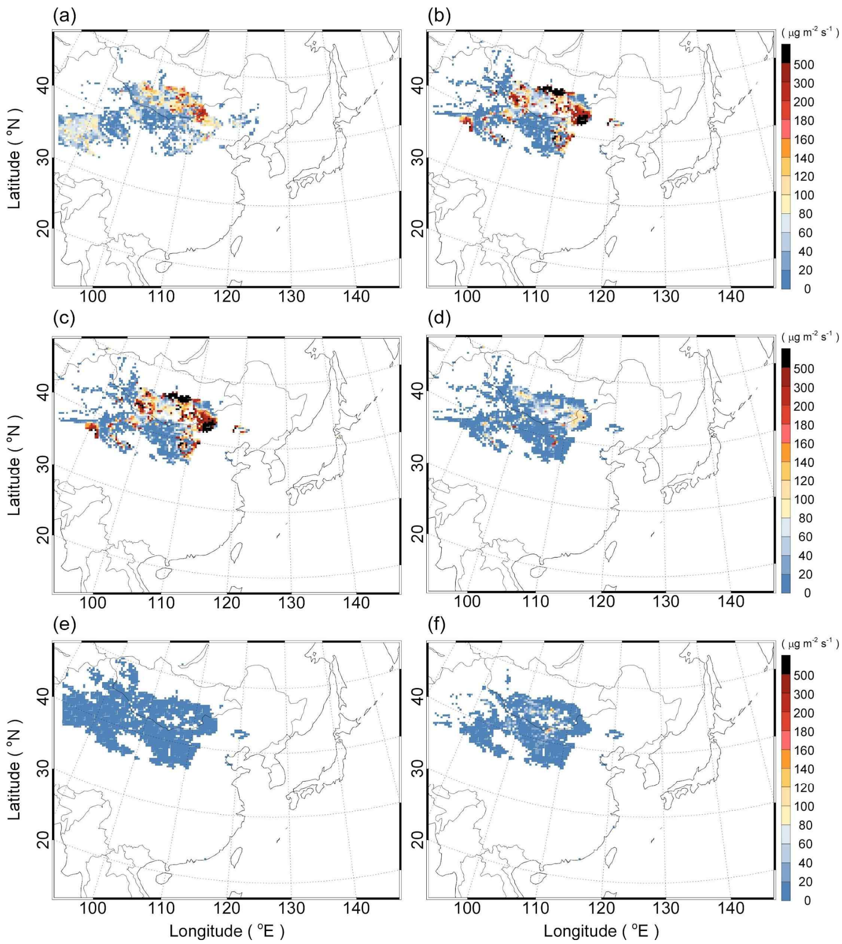

Figure 7. Horizontal distributions of the dust emission fluxes averaged during 20-23 February 2015 simulated by (a) new scheme, (b) UC01, (c) UC04, (d) UC11, (e) GO01, and (f) GA19.

https://doi.org/10.5194/egusphere-2026-4098
Preprint. Discussion started: 31 August 2026

This superior spatial representation was consistently maintained during the springtime Asian dust event from March 26 to 30, 2021 (Fig. 8). The new scheme dynamically captured the intensive dust outbreaks near northern China and inland Mongolia, showing an average dust emission flux of 36 μg m^{-2} s^{-1} (maximum of ~317 μg m^{-2} s^{-1}) (Fig. 8a). Most notably, the spatial distribution and the high-intensity emission fluxes simulated by the new scheme reasonably matched the dust plumes observed in the GK-2A/AMI dust RGB imagery. While the UC01 and UC04 schemes identified similar high-intensity source regions, their emission magnitudes were physically unrealistic, with maximums of 4213 and 5261 μg m^{-2} s^{-1}, respectively (Figs. 8b-c). Meanwhile, the UC11, GO01, and GA19 schemes remained largely underestimated to the severe meteorological forcing of the spring event, yielding weak and uniform distributions across the domain (Figs 8d–f). These spatial comparisons definitively confirm that the new semi-empirical scheme operates robustly across different seasons. By overcoming the extreme sensitivity issues and static source map limitations of previous schemes., the new scheme provides a highly reliable and dynamically accurate spatial distribution of East Asian dust emissions.

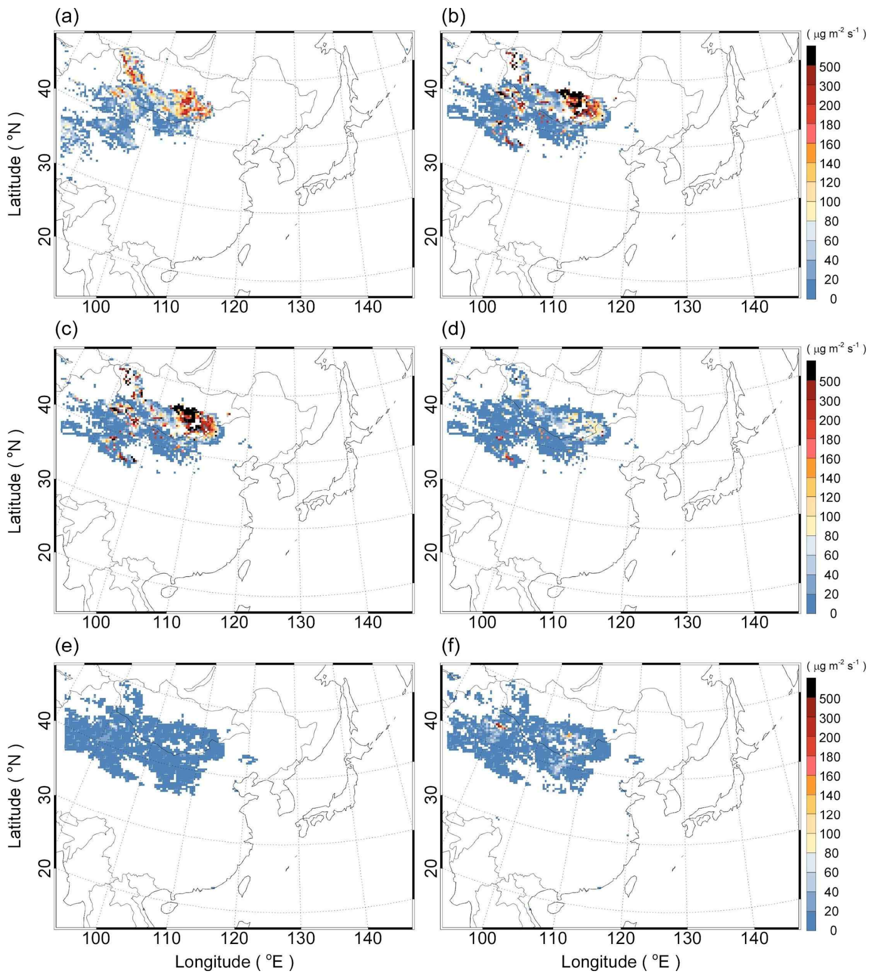

Figure 8. Horizontal distributions of the dust emission fluxes averaged during 26-30 March 2021 simulated by (a) new scheme, (b) UC01, (c) UC04, (d) UC11, (e) GO01, and (f) GA19.

https://doi.org/10.5194/egusphere-2026-4098
Preprint. Discussion started: 31 August 2026

5.4 Evaluation of near-surface PM_{10} concentrations

We evaluated the simulation performance of the new scheme by comparing the surface PM_{10} concentrations measured in the dust source area with the WRF-Chem simulation concentrations (Fig. 9). The UC01 and UC04 schemes showed significantly higher PM_{10} concentrations and were therefore scaled down by a factor of 10 for independent plotting clarity. The measured PM_{10} concentrations at Jurihe, Erenhot, and Erdene stations, located near the Gobi Desert, clearly captured the severe intensity of the Asian dust in the primary dust source regions (Figs. 9a-c). Although the simulated dust event in the new scheme persisted slightly longer than the observed duration, it successfully captured the peak PM_{10} concentration levels, which reached thousands of μg m^{-3}. On the other hand, the reference schemes showed extreme simulation performance with a clear tendency to over- or under-estimate the measured PM_{10} concentrations. In particular, while the simulated PM_{10} concentrations of the UC01 and UC04 schemes captured the timing of the peaks, their magnitudes reached tens of thousands of μg m^{-3}, overestimating the actual concentrations by more than a factor of three. The overestimation tendency of dust emission fluxes in the UC01 and UC04 schemes is driven by their high sensitivity to soil conditions. Conversely, the UC11, GO01, and GA19 schemes simulated PM_{10} concentrations below 1,000 μg m^{-3}, due to their characteristically weak dust emission fluxes and relatively low sensitivity to soil moisture. Consequently, they consistently demonstrated limitations in capturing the observed intensity of the Asian dust events.

The measured PM_{10} concentrations at the Naiman, Chifeng, and Tongliao stations, located near the Horqin Desert, clearly indicate the presence of Asian dust in the dust source region and along its transport path, albeit at lower concentration levels compared to those measured at Jurihe and Erenhot (Figs. 9d-f). Similar to their performance in the Gobi Desert, the UC01 and UC04 schemes tended to significantly overestimate the measurements, while the UC11, GO01, and GA19 schemes tended to underestimate them. Unlike these reference dust emission schemes, the newly developed dust emission scheme successfully captured the peaks of the measured PM_{10} concentrations across both the dust source and downwind transport regions. Most notably, the reference schemes failed to simulate any dust emissions at the Tongliao station because previously prescribed static dust source region map in the WRF-Chem model did not classify this area as a dust source region. In contrast, by incorporating an updated source region map, the new model correctly identified Tongliao as an active source region, successfully reproducing the measured PM_{10} concentrations (Fig. 9f). This definitive result demonstrates that the dynamically defined dust source region map for the East Asian region, along with the new dust emission scheme, is highly accurate and effectively resolves the blind spots of traditional static source maps.

https://doi.org/10.5194/egusphere-2026-4098
Preprint. Discussion started: 31 August 2026

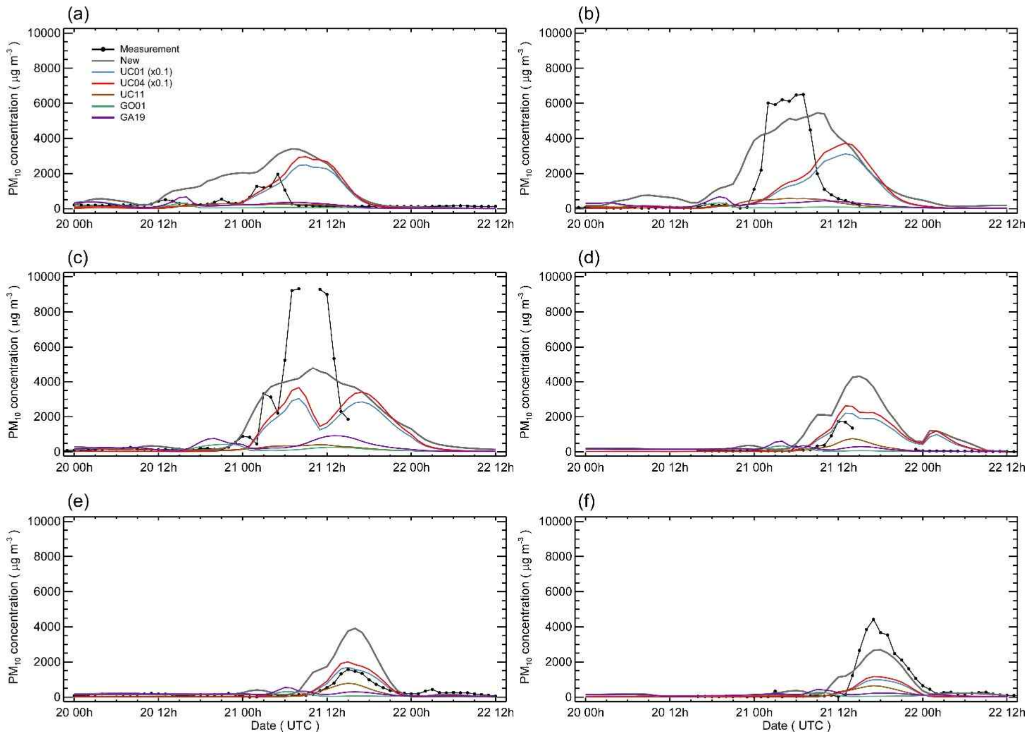

Figure 9. Comparison of the simulated and measured near-surface PM_{10} concentrations at the dust monitoring sites of (a) Erdene (near the Gobi Desert), (b) Erenhot, (c) Jurihe, (d) Chifeng, (e) Naiman, and (f) Tongliao (near the Horqin Desert) for 20-23 February 2015. The PM_{10} concentrations at the Naiman and Erdene monitoring towers were measured at a height of 3 m. Measurement data from Jurihe, Erenhot, Chifeng, and Tongliao stations were obtained from Park et al (2016b). Note that the concentrations simulated by the UC01 and UC04 schemes were scaled down by a factor of 10 for independent plotting clarity.

Figure 10 compares the simulated and measured near-surface PM_{10} concentrations at 10 monitoring stations operated by China Ministry of Ecology and Environment (MEE), distributed across the dust source and transport regions during the springtime event. Extremely high PM_{10} concentrations (up to ~10,000 μg m^{-3}) were measured at approximately 1200 UTC on March 27, making the onset of the Asian dust event. Subsequently, on March 28, PM_{10} concentrations of approximately 2,000 μg m^{-3} were measured at monitoring stations near the Shandong Peninsula in eastern China. Although the PM_{10} concentrations simulated by the newly developed model were slightly lower than the observed peaks at certain dust source region sites, the model accurately captured the overall magnitude peak timing, and duration of this severe dust event.

Consistent with the wintertime case, the UC01 and UC04 schemes captured the timing of the peaks but exhibited severe overestimation tendency, predicting unrealistic PM_{10} concentrations reaching tens of thousands of μg m^{-3}. Conversely, the UC11 and GO01 schemes largely failed to capture the intense PM_{10} concentrations measured in the dust source region, simulating severely underestimated values below 500 μg m^{-3}. The underestimation tendency by the UC11 scheme is primarily attributed to its sensitivity to the specific dust particle size distributions assigned to the loam soil textures prevalent in East Asia. The GA19 scheme simulated PM_{10} concentrations up to approximately 1,000 μg m^{-3}, which was significantly lower than the measured PM_{10} concentration levels. Notably, although GA19 calculates a higher total streamwise horizontal saltation flux than the new model, its final dust emission fluxes are significantly suppressed by the prescribed low erodibility factors (S) assigned to East Asia. This finding directly validates our methodological decision to completely remove the dependence on dust source strength functions in the new scheme. Because the performance of traditional dust schemes is heavily dictated by the choice of these static and often conflicting surface datasets (Lee and Lee, 2022), they inherently struggle to provide stable simulations for extreme Asian dust events. By utilizing optimized empirical coefficients and dynamically updated source

https://doi.org/10.5194/egusphere-2026-4098
Preprint. Discussion started: 31 August 2026

region maps, the new semi-empirical scheme successfully mitigates these input-driven instabilities, offering a far more robust predictive capability.

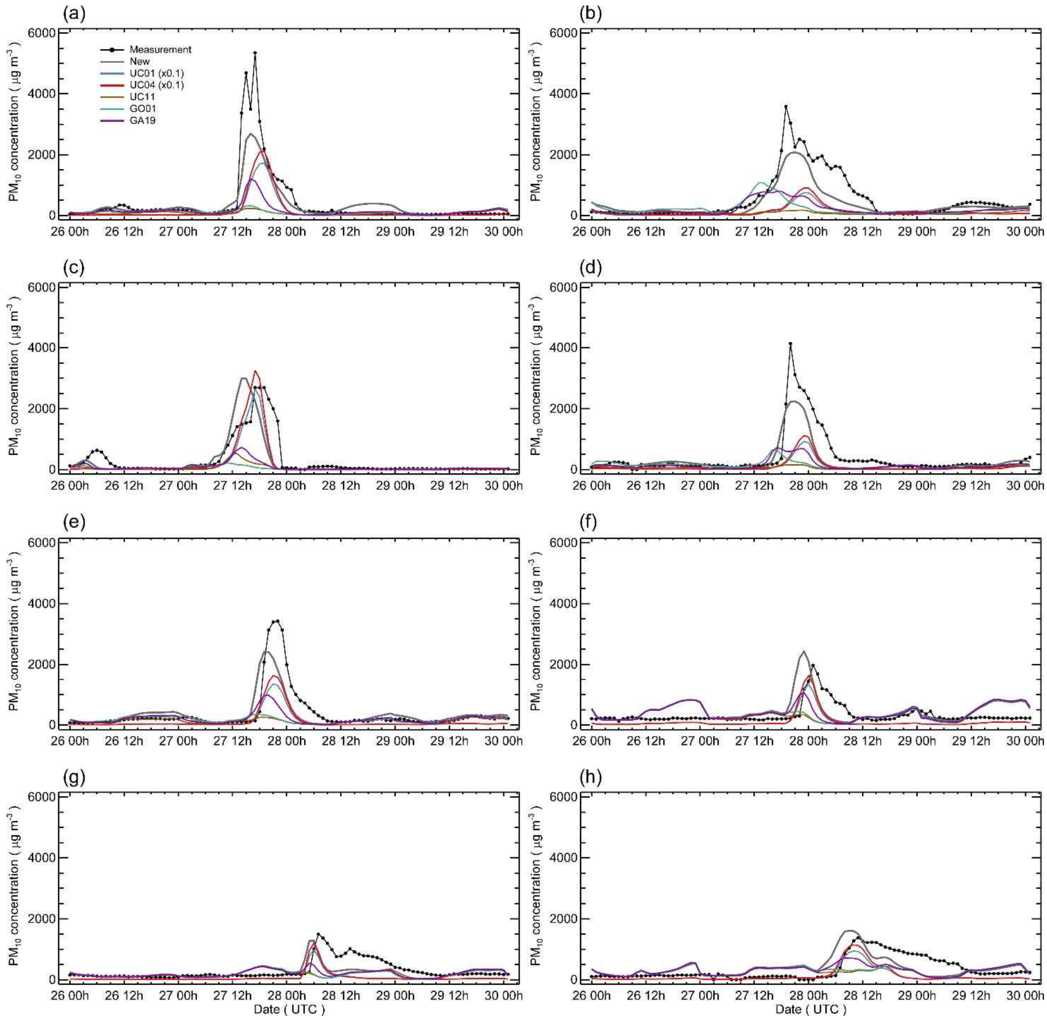

Figure 10. Comparison of the simulated and measured near-surface PM10 concentrations at the measurement stations of (a) S1 (2197A), (b) S2 (1949A), (c) S3 (2203A), (d) S4 (2638A), (e) S5 (2170A), (f) S6 (1030A), (g) S7 (1960A), (h) S8 (1655A) in the China's Ministry of Ecology and Environment (MEE) for 26-30 March 2021. Note that the concentrations simulated by the UC01 and UC04 schemes were scaled down by a factor of 10 for independent plotting clarity.

6 Conclusions

In this study, we developed and comprehensively evaluated a new semi-empirical dust emission scheme specifically optimized for the East Asian region. The new scheme establishes an advanced empirical relationship between dust emission flux and friction velocity by directly optimizing the comprehensive flux calculation equation against multi-level tower observations in the Horqin Desert. To support the accurate application of this relationship, we additionally improved the calculation process of the threshold friction velocity. This modified threshold friction velocity dynamically accounts for region-specific constraints−specifically, soil moisture cohesion, aerodynamic roughness drag partitioning, and snow cover fraction− while completely eliminating the conventional reliance on topography-based source strength functions. By deriving new optimal coefficients through the total dust emission flux equation combined with these refined physical parameters, the new

https://doi.org/10.5194/egusphere-2026-4098
Preprint. Discussion started: 31 August 2026

scheme directly and robustly captures the *in situ* dust emission mechanisms. When evaluated as a stand-alone box model, the new scheme successfully reproduced the observed dust emission fluxes. Crucially, it resolved the extremely high sensitivity to friction velocity and soil texture that severely degrades the performance of existing dust emission schemes, which exhibited flux variations of more than an order of magnitude depending on the specific soil type.

The newly developed scheme was subsequently implemented into the three-dimensional WRF-Chem model and evaluated against severe wintertime and springtime Asian dust events. Additionally, a dynamically updated natural dust source region map was also incorporated into the WPS system. The three-dimensional simulation results clearly demonstrated the superior predictive capability of the new model. While traditional dust schemes either produced extreme overestimations (UC01 and UC04) due to their vulnerability to surface input data uncertainties (e.g., vegetation fraction and soil moisture) or severely underestimated the events (UC11, GO01, and GA19), the new scheme accurately captured both the spatial distributions and the peak near-surface PM_{10} concentrations. Notably, the dynamic source region mapping enabled the new model to successfully reproduce dust plumes in previously unidentified blind-spot regions, such as the Manchurian Plain (e.g., the Tongliao station), which traditional schemes entirely missed.

Ultimately, this study proves that the semi-empirical scheme, where key parameters are derived by directly optimizing the comprehensive flux equation against *in situ* measurements, rather than relying on simple regressions between dust flux and friction velocity, provides a far more robust framework for simulating Asian dust than relying on highly sensitive, traditional empirical and physics-based schemes. Combined with dynamically updated surface boundary conditions, this new method effectively mitigates the extreme uncertainties driven by the over-reliance on static reduction factors and input data. While the optimal coefficients driving the current scheme were established under predominantly sandy soil conditions, future integration of flux estimations from sites with finer soil textures (e.g., clay-dominated regions like Erdene) will allow for further evaluation and generalization of the scheme. By successfully bridging the gap between local physical observations and regional modelling, the newly developed scheme significantly reduces simulation uncertainties driven by static input data, offering a highly reliable tool for operational Asian dust forecasting and environmental policy-making across East Asia.

https://doi.org/10.5194/egusphere-2026-4098
Preprint. Discussion started: 31 August 2026

Code availability. WRF-Chem v3.9.1 baseline source code is available for download at https://www2.mmm.ucar.edu/wrf/users/download/get_sources.html#WRF-Chem (last access: 28 June 2026). The source code for the Asian Dust Emission Scheme version 1.0 (ADES v1.0) implemented in WRF-Chem (v3.9.1) will be publicly open in a GitHub repository (https://github.com/LAEM4K/ADES4WRF) and also archived in Zenodo (https://doi.org/10.5281/zenodo.21272547).

Data availability. The Shuttle Radar Topography Mission (SRTM) 3 arc-second terrain elevation data (version 3), used to calculate the source strength function of the dust emission schemes, were obtained from NASA Earthdata (https://www.earthdata.nasa.gov/). The clay, silt, and sand fractions at the Naiman site were extracted from the RHWSD version 1.2 soil database (https://www.earthdata.nasa.gov/data/catalog/ornl-cloud-hwsd-1247-1). The 8-day averaged vegetation cover fraction from the GLASS-MODIS product was accessed via the THEIA platform (https://www.theia-land.fr/en/blog/product/series-of-vegetation-variables-avhrr/). Finally, the GLDAS version 2.1 snow depth and soil moisture data, provided at 3-hourly intervals, were sourced from NASA GES DISC (https://ldas.gsfc.nasa.gov/gldas).

Author contributions. JHL developed the experimental design and new dust emission scheme with SHL, curated and analyzed most of the data, and wrote the original draft as the primary author. SHL served as the corresponding author, assisting with review and editing of the original draft, data analysis, conceptualization, and funding acquisition. MSP and HZ provided data collection, analysis, and post-processing from the initial installation of the monitoring tower at the Naiman site in China. All co-authors critically reviewed the paper.

Competing interests. The authors declare that they have no conflict of interest.

Financial supports. This work was supported by the National Institute of Environmental Research (NIER) funded by the Ministry of Climate, Energy and Environment (MCEE) of the Republic of Korea (NIER-2024-03-03-002). JHL was supported by the National Research Foundation of Korea (NRF) grant, funded by the Ministry of Science and ICT (MSIT) of the Republic of Korea (RS-2026-25489516).

Acknowledgement. Primary WRF-Chem simulations were performed using the supercomputing resources of the National Center for Meteorological Supercomputer, Korea Meteorological Administration. Additional support was provided by the KREONET Advanced Research Program of KISTI. The authors thank the reviewers and the editor for their constructive comments, which significantly improved the manuscript.

https://doi.org/10.5194/egusphere-2026-4098
Preprint. Discussion started: 31 August 2026

References

Alfaro, S. C., Gaudichet, A., Gomes, L., and Maillé, M.: Modeling the size distribution of a soil aerosol produced by sandblasting, J. Geophys. Res. Atmos., 102, 11239–11249, https://doi.org/10.1029/97JD00403, 1997.

Bagnold, R. A.: The physics of blown sand and desert dunes, Chapmann and Hall, Methuen, London, 265 pp., 1941.

Carmichael, G.R., Calori, G., Hayami, H., Uno, I., Cho, S.Y., Engardt, M., Kim, S.-B., Ichikawa, Y., Ikeda, Y., Woo, J.-H., Ueda, H., and Amann, M.: The MICS-Asia study: model intercomparison of long-range transport and sulfur deposition in East Asia, Atmos. Environ., 36 (2), 175–199, https://doi.org/10.1016/S1352-2310(01)00448-4, 2002.

Chen, S., Yuan, T., Zhang, X., Zhang, G., Feng, T., Zhao, D., Zang, Z., Liao, S., Ma, X., Jiang, N., Zhang, J., Yang, F., and Lu, H.: Dust modeling over East Asia during the summer of 2010 using the WRF-Chem model, J. Quant. Spectrosc. Radiat. Transf., 213, 1–12, https://doi.org/10.1016/j.jqsrt.2018.04.013, 2018.

Chin, M., Rood, R.B., Lin, S.-J., Müller, J.-F., and Thompson, A.M.: Atmospheric sulfur cycle simulated in the global model GOCART: model description and global properties, J. Geophys. Res. Atmos., 105 (D20), 24671–24687. https://doi.org/10.1029/2000JD900384, 2000.

Dy, C. Y., and Fung, J. C. H.: Updated global soil map for the Weather Research and Forecasting model and soil moisture initialization for the Noah land surface model, J. Geophys. Res. Atmos., 121, 8777-8800, https://doi.org/10.1002/2015JD024558, 2016.

Dyer, A.J.: A review of flux-profile relationships, Bound-Lay Meteorol., 7, 363–372, 1974.

Fécan, F., Marticorena, B., and Bergametti, G.: Parametrization of the increase of the aeolian erosion threshold wind friction velocity due to soil moisture for arid and semi-arid areas, Ann. Geophys., 17, 149-157, https://doi.org/10.1007/s00585-999-0149-7, 1999.

Fountoukis, C., Ackermann, L., Ayoub, M. A., Gladich, I., Hoehn, R. D., and Skillern, A.: Impact of atmospheric dust emission schemes on dust production and concentration over the Arabian Peninsula, Model. Earth Syst. Environ., 2 (115), 1-6, https://doi.org/10.1007/s40808-016-0181-z, 2016.

Fratini, G., Ciccioli, P., Febo, A., Forgione, A., and Valentini, R.: Size segregated fluxes of mineral dust from a desert area of northern China by eddy covariance, Atmos. Chem. Phys., 7, 2839-2854, https://doi.org/10.5194/acp-7-2839-2007, 2007.

Gillette, D. A.: Fine particulate emissions due to wind erosion, Trans. ASAE., 20, 890-897, 1977.

Gillette, D. A., and Passi, R.: Modeling dust emission caused by wind erosion, J. Geophys. Res., 93, 14233-14242, https://doi.org/10.1029/JD093iD11p14233, 1988.

Ginoux, P., Chin, M., Tegen, I., Prospero, J. M., Holben, B., Dubovik, O., and Lin, S.-J.: Sources and distributions of dust aerosols simulated with the GOCART model, J. Geophys. Res. Atmos., 106, 20255-20273, https://doi.org/10.1029/2000JD000053, 2001.

Ginoux, P., Pospero, J. M., Gill, T. E., Hsu, N. C., and Zhao, M.: Global-scale attribution of anthropogenic and natural dust sources and their emission rates based on MODIS Deep Blue aerosol products, Rev. Gephys., 50, RG3005, https://doi:10.1029/2012RG000388, 2012.

Guenther, A., Karl, T., Harley, P., Wiedinmyer, C., Palmer, P.I., and Geron, C.: Estimates of global terrestrial isoprene emissions using MEGAN (model of emissions of Gases and aerosols from nature), Atmos. Chem. Phys., 6, 3181–3210, https://doi. org/10.5194/acp-6-3181-2006, 2006.

Han, L., Tsunekawa, A., and Tsubo, M.: Effect of frozen ground on dust outbreaks in spring on the eastern Mongolian Plateau, Geomorphology, 129, 412-416, https://doi.org/10.1016/j.geomorph.2011.03.005, 2011.

Han, T., Pan, X., and Wang, X.: Evaluating and improving the sand storm numerical simulation performance in Northwestern China using WRF-Chem and remote sensing soil moisture data, Atmos. Res., 251, 105411, https://doi.org/10.1016/j.atmosres.2020.105411, 2021.

https://doi.org/10.5194/egusphere-2026-4098
Preprint. Discussion started: 31 August 2026

Huang, J., Wang, T., Wang, W., Li, Z., and Yan, H.: Climate effects of dust aerosols over East Asian arid and semiarid regions, J. Geophys. Res. Atmos., 119 (19), 11398–11416, https://doi:10.1002/2014JD021796, 2014.

Imagawa, T., Fukuhara, M., and Wang, T.: A monitoring method of desertification in Naiman, Inner Mongolia, China, 111-116 pp., 2006.

Iversen, J. D., and White, B. R.: Saltation threshold on Earth, Mars and Venus, Sedimentology, 29, 111-119, https://doi.org/10.1111/j.1365-3091.1982.tb01713.x, 1982.

Ju, T., Li, X., Zhang, H., Cai, X., and Song, Y.: Effects of soil moisture on dust emission from 2011 to 2015 observed over the Horqin Sandy Land area, China, Aeolian Res., 32, 14-23, https://doi.org/10.1016/j.aeolia.2018.01.003, 2018.

Jugder, D.: A dust event in the Mongolian Gobi Desert in spring 2016: Observations and vertical dust flux estimation, E3S Web Conf., 99, 01009, https://doi.org/10.1051/e3sconf/20199901009, 2019.

Kim, D., Chin, M., Kemp, E. M., Tao, Z., Peters-Lidard, C. D., and Ginoux, P.: Development of high-resolution dynamic dust source function-A case study with a strong dust storm in a regional model, Atmos. Environ., 159, 11-25, https://doi.org/10.1016/j.atmosenv.2017.03.045, 2017.

Kim, J. E., Jung, W. S., Seo, W., Li, S., Oh, S. M., Shin, D., Ko, H.-J., Yoo, H.-J., Chung, C.-Y., and Kim, Y.-H.: Characteristics of Asian dust observed over the Yellow Sea during YES-AQ campaign in March, 2021 based on vessel and aircraft measurement, J. Korean. Soc. Atmos. Enrivon., 38, 557-576, h ttps://doi.org/10.5572/KOSAE.2022.38.4.557, 2022. (In English).

Kim, K.-M., Kim, S.-W., Choi, M., Kim, M., Kim, J., Shin, I., Kim, J., Chung, C-Y., Yeo, H., Kim, S.-W., Joo, S. J., McKeen, S. A., and Zhang, L.: Modeling Asian dust storms using WRF-Chem during the DRAGON Asia field campaign in April 2012, J. Geophys. Res. Atmos., 126, e2021JD034793, https://doi.org/10.1029/2021JD034793, 2021.

Kok, J. F., Mahowald, N. M., Fratini, G., Gillies, J. A., Ishizuka, M., Leys, J. F., Mikami, M., Park, M.-S., Park, S.-U., Van Pelt, R. S., and Zobeck, T. M.: An improved dust emission model-Part 1: Model description and comparison against measurements, Atmos. Chem. Phys., 14, 13023-13041, https://doi:10.5194/acp-14-13023-2014, 2014.

Kurosaki, Y., and Mikami, M.: Effect of snow cover on threshold wind velocity of dust outbreak, Geophys. Res. Lett., 31, https://doi:10.1029/2003GL018632, 2004.

LeGrand, S. L., Polashenski, C., Letcher, T. W., Creighton, G. A., Peckham, S. E., and Cetola, J. D.: The AFWA dust emission scheme for the GOCART aerosol model in WRF-Chem v3.8.1, Geosci. Model Dev., 12, 131-166, https://doi.org/10.5194/gmd-12-131-2019, 2019.

Lee, E.-H., and Park, S.-U.: A numerical simulation of an Asian dust (Hwangsa) event observed in Korea on March 10-12, 2004 using the modified ADAM model, Adv. Geosci., 5, 67-76, https://doi.org/10.1142/9789812707215_0009, 2006.

Lee, S.-S., Lim, Y.-K., Cho, J. H., Lee, H. C., and Ryoo, S.-B.: Improved dust emission reduction factor in the ADAM2 model using real-time MODIS NDVI, Atmosphere, 10, 702, https://doi:10.3390/atmos10110702, 2019.

Lee, J.-H., Chang, L.-S., and Lee, S.-H.: Simulation of air quality over South Korea using the WRF-Chem model: Impacts of chemical initial and lateral boundary conditions, Atmosphere, 25(4), 639–657, https://doi.org/10.14191/Atmos.2015.25.4.639, 2015. (In English).

Lee, J.-H., Lee, S.-H.: ADES4WRF (v1.0), Zenodo [code], https://doi.org/10.5281/zenodo.21272547, 2026.

Lee, J.-H., and Lee, S.-H.: Modeling a severe wintertime Asian dust event observed in the East Asia region: Sensitivity of the WRF Chem dust emission schemes, Atmos. Pollut. Res., 13, 101599, https://doi.org/10.1016/j.apr.2022.101599, 2022.

Lee, J.-H., Lee, S.-H., and Cho, J. H.: A novel method for detecting natural dust source regions using satellite and ground-based measurements, Atmos. Environ., 344, 121024, https://doi.org/10.1016/j.atmosenv.2024.121024, 2025.

https://doi.org/10.5194/egusphere-2026-4098
Preprint. Discussion started: 31 August 2026

Li, M., Zhang, Q., Kurokawa, J.-I., Woo, J.-H., He, K., Lu, Z., Ohara, T., Song, Y., Streets, D.G., Carmichael, G.R., Cheng, Y., Hong, C., Huo, H., Jiang, X., Kang, S., Liu, F., Su, H., and Zheng, B.: MIX: a mosaic Asian anthropogenic emission inventory under the international collaboration framework of the MICS-Asia and HTAP, Atmos. Chem. Phys, 17 (2), 935–963, https://doi.org/10.5194/acp-17-935-2017, 2017.

Marticorena, B., and Bergametti, G.: Modeling the atmospheric dust cycle: 1. Design of a soil-derived dust emission scheme, J. Geophys. Res. Atmos., 100, 16415–16430, https://doi.org/10.1029/95JD00690, 1995.

National Institute of Meteorological Research (NIMR): Asian Dust report. Research report, Seoul, Republic of Korea, 18 pp., 2008.

National Institute of Meteorological Sciences (NIMS): Asian Dust haze monitoring and prediction techniques. Jeju, Republic of Korea, 31-32 pp., 2015.

Park, M.-S., and Park, S.-U.: Effects of topographical slope angle and atmospheric stratification on the surface-layer turbulence, Bound. Lay. Meteor., 118, 613-633, https://doi.org/10.1007/s10546-005-7206-x, 2006.

Park, M.-S., Park, S.-U., and Chun, Y.: Improved parameterization of dust emission (PM10) fluxes by the gradient method using the Naiman tower data at the Horqin desert in China, Sci. Total Environ., 412, 265-277, https://doi:10.1016/j.scitotenv.2011.09.068, 2011a.

Park, S.-U., and In, H.-J.: Parameterization of dust emission for the simulation of the yellow sand (Asian dust) observed in March 2002 in Korea, J. Geophys. Res. Atmos., 108, 4618, https://doi.org/10.1029/2003JD003484, 2003.

Park, S.-U., Choe, A., Lee, E.-H., Park, M.-S., and Song, X.: The Asian Dust Aerosol Model 2 (ADAM2) with the use of normalized difference vegetation data (NDVI) obtained from the spot4/vegetation data, Theor. Appl. Climatol., 101, 191-208, https://doi.org/10.1007/s00704-009-0244-4, 2010a.

Park, S.-U., Park, M.-S., and Chun, Y.: Asian dust events observed by a 20-m monitoring tower in Mongolia during 2009, Atmos. Environ., 44, 4964-4972, https://doi.org/10.1016/j.atmosenv.2010.08.014, 2010b.

Park, S.-U., Park, M.-S., and Chun, Y.: A parameterization of dust concentration (PM10) of dust events observed at Erdene in Mongolia using the monitored tower data, Sci. Total Environ., 409 (15), 2951–2958, https://doi.org/10.1016/j.scitotenv.2011.04.024, 2011b.

Park, S.-U., Ju, J.-W., Lee, I.-H., and Joo, S. J.: A parameterization of dust emission (PM10) fluxes of dust events observed at Naiman in Inner Mongolia using the monitored tower data, Atmos. Environ., 140, 420-431, http://dx.doi.org/10.1016/j.atmosenv.2016.06.004, 2016a.

Park, M. E., Cho, J.H., Kim, S., Lee, S.-S., Kim, J.E., Lee, H.C., Cha, J.W., and Ryoo, S.B.: Case study of the heavy Asian dust observed in late February 2015, Atmosphere, 26 (2), 257–275, https://doi.org/10.14191/Atmos.2016.26.2.257, 2016b. (In English).

Raupach, M.: Drag and drag partition on rough surfaces, Bound. Lay. Meteor., 60, 375-395, https://doi.org/10.1007/BF00155203, 1992.

Shao, Y.: A model for mineral dust emission, J. Geophys. Res. Atmos., 106, 20239-20254, https://doi.org/10.1029/2001JD900171, 2001.

Shao, Y.: Simplification of a dust emission scheme and comparison with data, J. Geophys. Res. Atmos., 109, https://doi.org/10.1029/2003JD004372, 2004.

Shao, Y., Raupach, M. R., Findlater, P. A.: Effect of saltation bombardment on the entrainment of dust by wind, J. Geophys. Res., 98, 12719-12726, https://doi.org/10.1029/93JD00396, 1993.

Shao, Y., Raupach, M. R., and Leys, J. F.: A model for predicting aeolian sand drift and dust entrainment on scales from paddock to region, Aust. J. Soil Res., 34, 309-342, https://doi.org/10.1071/SR9960309, 1996.

Shao, Y., Ishizuka, M., Mikami, M., and Leys, J. F.: Parameterization of size-resolved dust emission and validation with measurements, J. Geophys. Res. Atmos., 116, https://doi.org/10.1029/2010JD014527, 2011.

https://doi.org/10.5194/egusphere-2026-4098
Preprint. Discussion started: 31 August 2026

Shinn, E.A., Smith, G.W., Prospero, J.M., Betzer, P., Hayes, M.L., Garrison, V., and Barber, R. T.: African dust and the demise of Caribbean coral reefs. Geophys, Res. Lett., 27 (19), 3029–3032, https://doi.org/10.1029/2000GL011599, 2000.

Stockwell, W.R., Kirchner, F., Kuhn, M., and Seefeld, S.: A new mechanism for regional atmospheric chemistry modelling, J. Geophys. Res. Atmos., 102 (D22), 25847–25879, https://doi.org/10.1029/97JD00849, 1997.

Su, L., and Fung, J. C. H.: Sensitivities of WRF-Chem to dust emission schemes and land surface properties in simulating dust cycles during springtime over East Asia, J. Geophys. Res. Atmos., 120, 11215-11230, https://doi.org/10.1002/2015JD023446, 2015.

Sun, J., Zhang, M., and Liu, T.: Spatial and temporal characteristics of dust storms in China and its surrounding regions, 1960-1999: Relations to source area and climate, J. Geophys. Res. Atmos., 106(D10), 10325-10333, https://doi.org/10.1029/2000JD900665, 2001.

Uno, I., Wang, Z., Chiba, M., Chun, Y. S., Gong, S. L., Hara, Y., Jung, E., Lee, S.-S., Liu, M., Mikami, M., Music, S., Nickovic, S., Satake, S., Shao, Y., Song, Z., Sugimoto, N., Tanaka, T., and Westphal, D. L.: Dust model intercomparison (DMIP) study over Asia: Overview, J. Geophys. Res., 111(D12213), https://doi:10.1029/2005JD006575, 2006.

Wang, L., Shi, Z. H., Wu, G. L., and Fang, N. F.: Freeze/thaw and soil moisture effects on wind erosion, Geomorphology, 207, 141-148, http://dx/doi.org/10.1016/j.geomorph.2013.10.032, 2014.

Wang, X., Zhao, X., Li, Y., Zuo, X., Cui, D., Qu, H., and Lian, J.: Responses of soil respiration to simulated precipitation and Nitrogen, Phosphorus additions in Horqin sandy Land of northeastern China, Fresen. Environ. Bull., 22, 1463-1471, 2013.

Wang, X., Cai, D., Li, D., Lou, J., Zheng, Y., Hu, S., and Liu, F.: Dust deposition and its significance to soil nutrients in the Otindag desert, China, J. Arid Environ., 194 (104612), https://doi.org/10.1016/j.jaridenv.2021.104612, 2021.

Westphal, D. L., Toon, O. B., and Carlson, T. N.: A two-dimensional numerical investigation of the dynamics and microphysics of Saharan dust storms, J. Geophys. Res., 92, 3027-3049, https://doi.org/10.1029/JD092iD03p03027, 1987.

White, B. R.: Soil transport by winds on Mars, J. Geophys. Res., 84, 4643-4651, https://doi.org/10.1029/JB084iB09p04643, 1979.

Woodruff, N.P., and Siddoway, F. A.: A wind erosion equation, Soil Sci. Soc. Am. J., 29, 602-608, 1965.

Yuan, W., and Zhang, J.: High correlations between Asian dust events and biological productivity in the western North Pacific, Geophys. Res. Lett., 33 (7), L07603, https:// doi.org/10.1029/2005GL025174, 2006.

Yuan, T., Chen, S., Huang, J., Zhang, X., Luo, Y., Ma, X., and Zhang, G.: Sensitivity of simulating a dust storm over Central Asia to different dust schemes using the WRF-Chem model, Atmos. Environ., 207, 16–29, https://doi.org/10.1016/j.atmosenv.2019.03.014, 2019.

Zender, C. S., Bian, H., and Newman, D.: Mineral Dust Entrainment and Deposition (DEAD) model: Description and 1990s dust climatology, J. Geophys. Res. Atmos., 108 (D14), 4416, https://doi.10.1029/2002JD002775, 2003.

Zhang, H., Zhu, H., Peng, Y., Kang, L., Chen, J., and Park, S.-U.: Experiment on dust flux during dust storm periods over desert area, Acta. Meteorol. Sin., 22, 239-247, 2008.

Zhao, H.-L., Zhou, R.-L., Su, Y.-Z., Zhang, H., Zhao, L.-Y., and Drake, S.: Shrub facilitation of desert land restoration in the Horqin sand land of Inner Mongolia, Ecol. Eng., 31, 1-8, https://doi.org/10.1016/j.ecoleng.2007.04.010, 2007.

Zhao, J., Ma, X., Wu, S., and Sha, T.: Dust emission and transport in Northwest China: WRF-Chem simulation and comparisons with multi-sensor observations, Atmos. Res., 241, 104978, https://doi.org/10.1016/j.atmosres.2020.104978, 2020.

Zhou, W., Wang, H., and Ge, Q.: Contributions of climatic factors and vegetation cover to the temporal shift in Asian dust events, npj Clim. Atmos. Sci., 7, 328, https://doi.org/10.1038/s41612-024-00887-9, 2024.

https://doi.org/10.5194/egusphere-2026-4098
Preprint. Discussion started: 31 August 2026

Zhou, Z., and Zhang, G.: Typical severe dust storms in Northern China during 1954-2003, Chin. Sci. Bull., 48, 2366-2370, https://doi:10.1360/03wd0029, 2003.